American Mineralogist, Volume 90, pages 701–707, 2005

Charge contrast imaging of fine-scale microstructure and compositional variation in garnet using the environmental scanning electron microscope

SIMON J. CUTHBERT[1,*] AND JAMES O. BUCKMAN[2]

[1]School of Engineering and Science, University of Paisley, Paisley PA1 2BE, U.K.
[2]Institute of Petroleum Engineering, Heriot-Watt University, Edinburgh EH14 4AS, U.K.

ABSTRACT

Gaseous secondary electron (GSE) imaging of eclogite garnets under the environmental scanning electron microscope (ESEM) at low chamber gas pressures reveals detailed image contrast patterns (charge-contrast images, CCI) that are not present in back-scattered or secondary electron images. Image intensity is a function of the amount of surface charge accumulation. Successful acquisition of CCI depends on frame size and beam scan rate at a given chamber gas pressure and beam current. Images are obtained in a few seconds, and are stable and reproducible. CCI patterns do not correlate with cracks or grain boundaries, but do correspond closely to variations in major-element composition, both in the form of concentric (growth) zoning, and branching, linear features interpreted as cracks that have been healed by new garnet growth. Causes of CCI are not yet well understood, but may be related to variations in lattice defect density and their influence on charge-trapping and dissipation. These in turn influence the rate of charge build-up at or very close to the specimen surface. One interesting possibility is that CCI images detect vacancies related to non-homovalent coupled substitutions involving, for example, REE and hydroxyl, so the method offers a way of imaging the distribution of these trace species in garnets. The CCI images are rich in microstructural detail and offer the potential for rapid, high-resolution, low-noise reconnaissance mapping of intragranular microstructure and compositional variation in both natural and synthetic garnets.

INTRODUCTION

Natural aluminosilicate garnets are well known to exhibit internal compositional and microstructural features that are potentially rich in information about the petrological and deformation history of their host rocks (Hirsch et al. 2003; Hwang et al. 2001; Matsyuk et al. 1998; Matthews et al. 1992; Prior et al. 2000; Spear and Daniel 1998; Terry and Heidelbach 2004; Trepmann and Stockhert 2002). Garnets are also important materials in magneto-ceramics and lasers. Thus, imaging of compositional variation and defect structures in synthetic garnet is important in the development of improved material quality and novel industrial applications (e.g., Zamoryanskaya and Pis'mennyi 2000). However, fine-scale variability of composition, defect density, and lattice orientation is usually invisible under the polarizing optical microscope, and may even be invisible to back-scattered electron (BSE) imaging on ordinary scanning electron microscopes (SEM). High-resolution X-ray compositional mapping on an SEM or electron microprobe is time-consuming. It would be useful to have a rapid reconnaissance imaging method for investigation of fine-scale internal variability of garnet. Cathodoluminescence (CL) imaging fulfills this role for some silicates: normal CL detectors generally do not detect luminescence contrasts in common pyralspite garnets, although hot-cathode luminescence microscopy has recently been reported to exhibit internal variation in garnet, such as compositional zoning and healed microcracks (Schertl 2003).

Watt et al. (2000) have reported image contrast on uncoated, polished sections of natural silicates using a gaseous secondary electron detector (GSED) on an environmental scanning electron microscope (ESEM). These charge-contrast images (CCI) result from variable surface charge accumulation and dissipation, and closely resemble CL images for luminescent silicates such as quartz and zircon, suggesting a related causal mechanism. However, Watt et al. (2000) have shown that CCI is also possible for silicates that are not normally luminescent, such as cordierite and micas. They considered that this method has particular value in detecting the effects of otherwise cryptic, fluid-related alteration. Encouraged by these results, we have investigated the CCI characteristics of natural pyralspite garnets under the ESEM, and have found that it is possible to image fine-scale internal structure and compositional variation rapidly and conveniently, making it potentially very useful in reconnaissance studies of garnet microstructures. The purpose of this paper is to report our preliminary findings on the charge-contrast image characteristics of garnets, to make some initial deductions about their microstructural and crystal-chemical causes, and to highlight the potential usefulness of this technique for garnet studies in the mineralogical and materials sciences.

METHODOLOGY

The environmental scanning electron microscope (ESEM), or variable-pressure electron microscope, is capable of imaging specimens of insulating materials without the requirement for

* E-mail: simon.cuthbert@paisley.ac.uk

0003-004X/05/0004–701$05.00/DOI: 10.2138/am.2005.1572

a conductive coating. This is possible because the specimen chamber is filled with a gas (normally water vapor or nitrogen). The gas is ionized by the electron beam, or by energetic back-scattered electrons from the specimen surface. Positively charged gas molecules are attracted toward the specimen surface, where they neutralize charge deposited there by the electron beam. Secondary electrons emerging from the specimen surface, or from a few nanometers below the surface, interact with the chamber gas, which create an amplification effect so that a cascade of secondary electrons flows toward the positively biased GSED (Mohan et al. 1998). The GSED signal is then combined with the beam raster position to create a gaseous secondary (GSE) image. Several studies have found that if the beam current, beam scan rate, and gas pressure are balanced at certain levels, a residual charge can be left at or just below the specimen surface that influences the intensity of the GSE image. Variations in the image intensity (image contrasts) have been observed that often have either a concentric arrangement, and hence may be related to crystal-growth-related features (Baroni et al. 2000; Griffin 1997, 1998, 2000), or take the form of linear, branching features that may be healed cracks or planar concentrations of lattice defects (Watt et al. 2000). In this way, CCI have similarities with CL images (Griffin 1998, 2000). The physical basis for the charge contrast is still poorly understood. An early study of charge-sensitive SE imaging on synthetic diamond attributed image contrast to charge channeling along intracrystalline defects and grain boundaries (Harker et al. 1994). Griffin et al. (2000) and Watt et al. (2000), in studies of gibbsite, silicates, and sulfides, developed a model in which trapped, implanted charge influences emission of secondary electrons produced at the specimen surface due to interaction with the electron beam ("SE1" of Watt et al. 2000). Electrons implanted in the mineral surface normally dissipate rapidly, but in some cases, they may move in valence or conduction bands and become trapped at intrinsic lattice defects. Concentration of charge at defects below the specimen surface may result in enhancement of SE1 emission above it. Under normal operating conditions, the flood of positive ions to the specimen surface suppresses all SE1 emission, so that images are dominated by SE generated by exiting back-scattered electrons (BSE), or by ionizing collisions of BSE with the chamber gas (SE2 of Watt et al. 2000). However, Griffin (1998) suggested that if the chamber gas pressure is reduced, and beam current, working distance, and scan rates adjusted accordingly, SE1 will dominate and GSE image contrast influenced by differential charge trapping will become visible. In short, CCI reflect variations in charge dissipation of relatively wide band-gap insulating materials. Images are stable and reproducible, but contrast may be reversed by changing scan rate, apparently due to spatial differences in the time constants for charge trapping vs. dissipation (Watt et al. 2000). The signal is thought to originate in the uppermost few nanometers of the specimen surface, and the very small activation volume for the signal gives CCI images a greater spatial resolution than CL or BSE images (Griffin 2000).

We investigated garnets from an eclogite at Krokeneset, Nordfjord, Norway (UTM ref. 32VLP085702). Garnets from this eclogite body are known to exhibit concentric compositional zoning (Bryhni and Griffin et al. 1971), and cataclastic deformation (Carswell et al. 2003; Cuthbert and Carswell 2003). We were interested to see whether charge contrast imaging could resolve growth-related features similar to those reported by Griffin (1997, 1998, 2000) in synthetic gibbsite, and the healed crack features found in biotite and cordierite by Watt et al. (2000). Standard 30 μm polished thin sections were manufactured by lapping in various alumina grits on a Logitech PM2 grinding lap, followed by polishing with diamond paste, finishing with a 0.25 micrometer grit size. The slide was washed in distilled water and acetone to remove surface contamination from the polishing process, because CCI is known to image surface impurities (Griffin 2000). CCI was carried out in a Philips-FEI XL30 ESEM at the Centre for Environmental Scanning Electron Microscopy, Institute of Petroleum Engineering, Heriot-Watt University. Accelerating voltage was 20 kV for all observations at working distances of 9.9–10.3 mm. Water vapor was used as the chamber gas at a pressure of 0.4 Torr.

The best image contrast was achieved at relatively slow beam-scan rates, with line-scan times of 1.68 to 40 ms. Scan rate for successful imaging had to be varied as magnification was changed, with lower magnifications requiring slower scan rates. This is because the scan rate controls the rate of deposition of charge onto the specimen surface. In order to maintain a charge density sufficient to produce an image, the optimum line scan time for a larger image frame (lower magnification) is greater than for a small image frame, given that beam current, gas pressure, and working distance are held constant. For example, a line time of 40 ms gave good images at magnifications of 40× and 49×, but at 79× showed only surface polishing artifacts, and at 99× showed no contrast. At 99× magnification, a good contrast image was produced at a line time of 6.73 ms, but no contrast was observed at 1.68 and 40 ms.

Compositional maps of the garnets studied under the ESEM were acquired for comparison with the CCI images. Small-area, high-resolution compositional maps for Ca, Fe, Mg, and Mn were acquired on a Hitachi S4100 field emission SEM at the University of Paisley Thin Film Centre, using an Oxford Instruments ISIS energy dispersive X-ray spectrometer with a germanium detector with accelerating voltage 20kV, at a working distance of 15 mm. Whole-garnet maps for the same set of elements were acquired on a Cameca SX50 wavelength-dispersive electron microprobe at the Bayreuth GeoInstitut, Germany, with accelerating voltage of 20kV and a beam current of 20nA. Images were adjusted on ImageJ image processing software to give the best possible contrast. As a result of this, count rates are not directly comparable between images.

RESULTS

The eclogite studied here has two distinct garnet grain-size populations, with abundant smaller grains ca. 1 mm in diameter and a few grains up to 6.5 mm, commonly concentrated in quartz-rich layers. Most grains exhibit concentric color zoning in thin section under the polarizing microscope, with darker red cores and narrow, paler red rims. Garnets from this eclogite body commonly show porphyroclastic textures. One small grain, part of a larger grain, and one entire large grain are described here.

The small garnet is partially embedded in the rim of a large grain (Figs. 1–4). BSE images are shown in Figures 1b, 1d, and 1f, and conventional SE images in Figures 2, 3, and 4. These

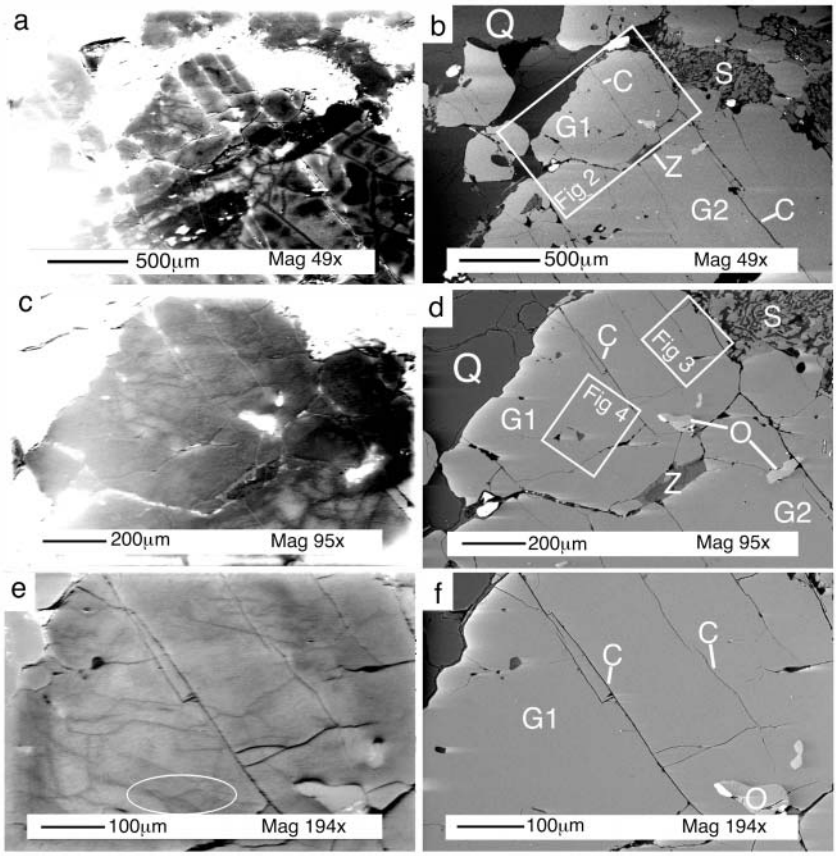

FIGURE 1. ESEM images of a small garnet (G1) partially embedded in a larger garnet (G2). For all images, accelerating voltage was 20 kV, vacuum 0.4 Torr, and working distance 10.2–10.8mm. Note that "mag" in the scale boxes indicates machine magnification and not actual image magnification. (**a**, **c**, **e**) Charge-contrast images at machine magnifications of 49×, 95×, and 191×, respectively. Garnet in shades of gray to black, bright areas are quartz and diopside-plagioclase symplectite. White oval in **e** points to branching charge-contrast features corresponding to those in the Ca image in Figure 4. (**b**, **d**, **f**) BSE images of the areas imaged in **a**, **c**, **e** respectively. Garnet (G1, G2) is pale gray, with paler gray inclusions of omphacite (O) and white rutile. Quartz matrix (Q) darker gray. Fine pale gray / dark gray intergrowths are diopside-plagioclase symplectites (S). A single medium-gray zoisite grain (Z) lies along the grain boundary of G1 and G2. Cracks in the slide surface show as black lines (C) — note the corresponding linear features in the CCI images. White box in **b** shows small garnet covered by compositional maps in Figure 2. Right-hand white box in **d** shows area near garnet rim covered in Figure 3; left-hand box shows area in garnet core covered by Figure 4.

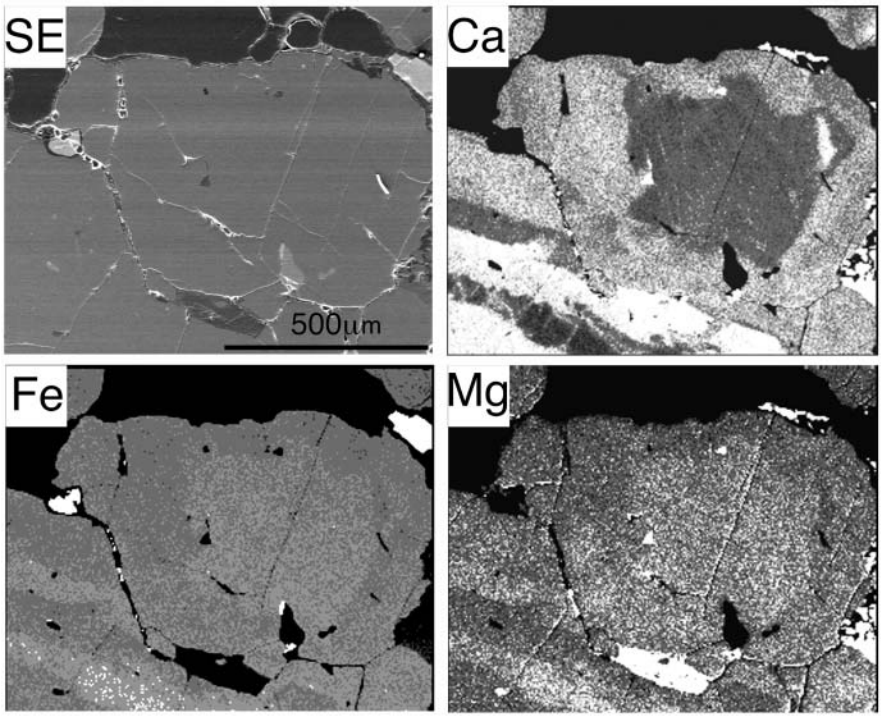

FIGURE 2. Conventional secondary electron (SE) image of small garnet (top left), and high-resolution X-ray compositional maps for Ca, Fe, and Mg of the same area.

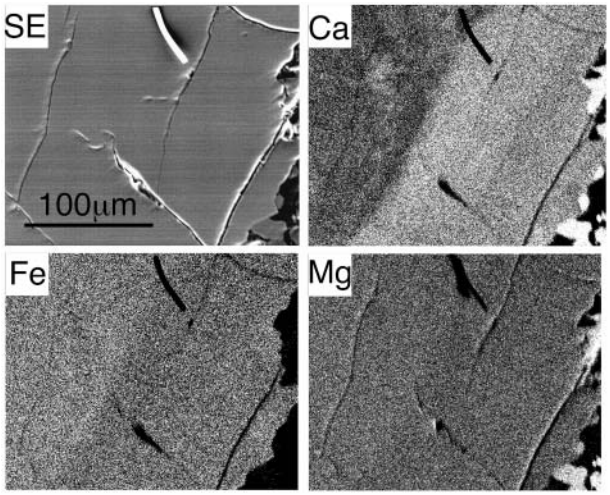

FIGURE 3. Conventional secondary electron (SE) image (top left) of rim area in the small garnet shown in Figures 1 and 2, and high-resolution X-ray compositional maps for Ca, Fe, and Mg of the same area. Short line feature at center top is a small hair on the slide surface.

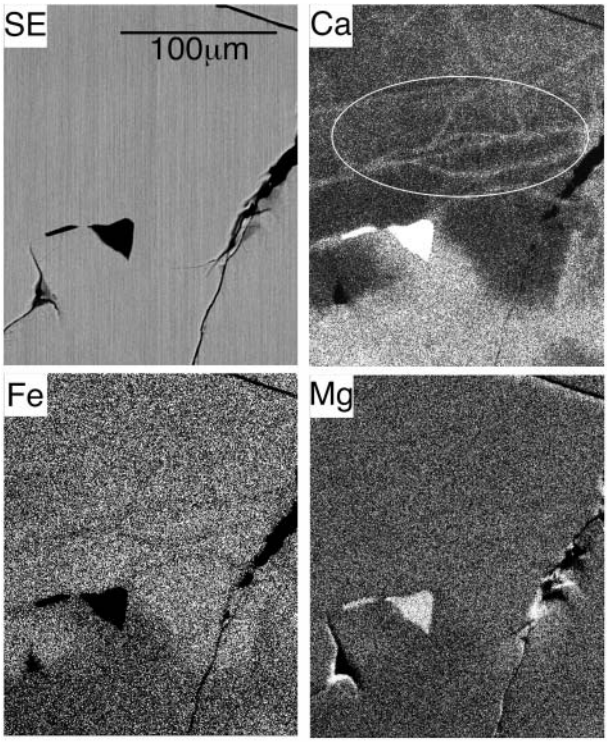

FIGURE 4. Conventional secondary electron (SE) image (top left) of part of the core of the small garnet shown in Figure 2 and high-resolution X-ray compositional maps for Ca, Fe, and Mg of the same area. White oval in the Ca image points to the branching high-Ca features corresponding to the identical CCI-dark feature in Figure 1e.

images were collected on both the ESEM and cold-field emission SEM, and show the presence of fractures cutting the garnet and inclusions of other phases, but otherwise lack variation in image intensity. However, CCI images from the ESEM show clear and highly detailed image contrast (Figs. 1a, 1c, and 1e). At the lowest magnification of 45× (Fig. 1a), the very bright intensity of the surrounding quartz and plagioclase-diopside symplectite rather overwhelms the image. Nevertheless, clear variations in charge contrast can be seen in the garnet. Cracks observed as black lines under BSE and SE show as bright lines in CCI, but in the coherent garnet between these cracks a network of anastomosing fine, dark lines is visible. In addition, the small, idioblastic garnet grain (marked G1 in Figs. 1b, 1d, and 1f) near the center of the field shows a concentric zoning, with a brighter gray core and a paler rim. Note also the two very dark strips, merging at their right-hand ends, at the rim of the larger garnet (G2) in which the smaller grain is embedded. At 95× magnification (Fig. 1c), these features can be seen rather more clearly, and the cracks are not so bright in this CCI. At 191× magnification (Fig. 1e), the surrounding quartz is almost eliminated from the frame, so the image contrast is dominated by variation within garnet: the concentric and branching patterns are clearly visible. Here, the cracks have reversed their CCI image contrast and appear as dark lines. This contrast reversal has happened at the fastest line scan rate (1.68 μs per line). Contrast reversal is commonly found in CCI imaging and has been attributed by Watt et al. (2000) to the influence of differences in the time constant for charge dissipation as beam scan rate (i.e., charge build-up rate) is varied.

Figure 2 shows compositional maps for Ca, Fe, and Mg, and a conventional SE image of the small garnet (G1) and part of its larger host garnet (G2). As indicated by optical color zoning, the garnet G1 shows a clear concentric compositional zoning in Mg, Fe, and especially Ca (Mn showed no discernable variation). The concentric zoning in the CCI images shows a strong correspondence to the concentric compositional zoning pattern, which is most obvious in the Ca map. Image intensity in the CCI image shows a good inverse correlation with Ca concentration, and a positive correlation with Fe and Mg. Concentric zoning of this type in the outer parts of garnets from Nordfjord eclogites, showing radially increasing Mg/Fe has commonly been attributed to new, eclogite-facies garnet growth around a core of old, amphibolite-facies garnet (Bryhni and Griffin 1971; Krogh 1982; Carswell et al. 2003; Carswell and Cuthbert 2003), although the higher Ca rim is unusual, as Ca is generally found to decrease outward in the Nordfjord eclogites. The two dark strips on the GSE image in the edge of the adjacent large garnet (G2) exactly match two very Ca-rich strips (Fig. 2).

Figure 3 shows the concentric compositional zoning in more detail, and reinforces the correspondence between the dark CCI rim and the position of the Ca-richer, Fe- and Mg-poorer rim. In Figure 4, an ultrafine resolution compositional map for Ca shows exact correspondence of the dark, anastomosing line features in CCI to lines higher in Ca (Fig. 4). Very faint, dark, low-Fe lines can be seen in the same positions (Fig. 4). Note that these features are unrelated to the cracks in the garnet, as seen in the conventional SE image (Fig. 2). The line features do, however, exhibit a pattern resembling an array of fractures, and could be interpreted as cracks healed by growth of new garnet. The crack-sealing garnet has a similar composition to the eclogite-facies rim-zone garnet, so presumably grew under eclogite-facies conditions. Matthews at al. (1992) interpreted similar features in garnets from mantle peridotites, in this case

imaged by high-contrast BSE, to be healed cracks. They noted a close correspondence of BSE image contrast with compositional variation, the linear BSE features matching increases in Fe and Ti, and decreases in Mg (Ca showed no variation in this case). Trace-element variations were also found to correspond to these features, including Y, Zr, and the REE. In another specimen from the same xenolith suite, Prior et al. (2000) found a similar, cellular structure with crack-like features in garnets that proved to be arrays of dislocations associated with a darker BSE signal that they attributed to different garnet composition. The main difference with the case described here is that we observed no BSE image contrast.

Matthews et al. (1992) attributed the linear features in their peridotite garnets to metasomatic effects of melts penetrating along cracks, which were then sealed by precipitation of new garnet. Prior et al. (2000) attributed their observations to crystal-plastic deformation and associated changes to diffusional characteristics that aided compositional re-equilibration. Watt et al. (2000) attributed similar GSE, CCI features in cordierite and biotite to the action of metasomatizing fluids. There is no evidence for melting in the Krokeneset eclogite, but a metasomatic influence may have acted to form the linear GSE features.

Figure 5a is a Ca compositional map of a large garnet from the same thin section as those described above. Note that the garnet shows a network of narrow Ca-rich seams that is densest close to the grain margin. Variations in Mg and Fe show an identical spatial variation, with the seams having lower Fe and Mg (but higher Mg/Fe) and lower Mn. A narrow overgrowth shows the same composition as the seams. The broadest seam is partly cored by quartz (Q) and omphacite (O) (Fig. 5a). GSE images show dark lines that correspond exactly to the Ca-rich seams (Figs. 5c and 5e). These curvilinear features are again interpreted to be sealed cracks, but in this case the quartz and omphacite crack fills are considered to have been precipitated by a fluid that penetrated the cracks under eclogite-facies conditions. The garnet crack-seals are also inferred to have precipitated by the action of this fluid. Hence, in line with the conclusions of Watt et al. (2000), the action of a metasomatic fluid is inferred to have contributed to the formation of the curvilinear features observed on the GSE image. It is noteworthy that the broad Ca-rich seam to the left of the quartz vein in Figure 5a is not entirely followed by the dark band on the GSE images (Fig. 5c and 5e)—the GSE band fades out whereas the compositional band continues to the edge of the grain. Hence, it is possible that Ca, Fe, Mg, or Mn are not directly responsible for the GSE image contrast, but some other factor operated that was normally, but not always, coincident with the major-element variation. A distinct closed loop in the CCI images (Figs. 5c and 5e) is absent in the compositional map (Fig. 5a), possibly due to limitations in the spatial or compositional resolution of the microprobe mapping.

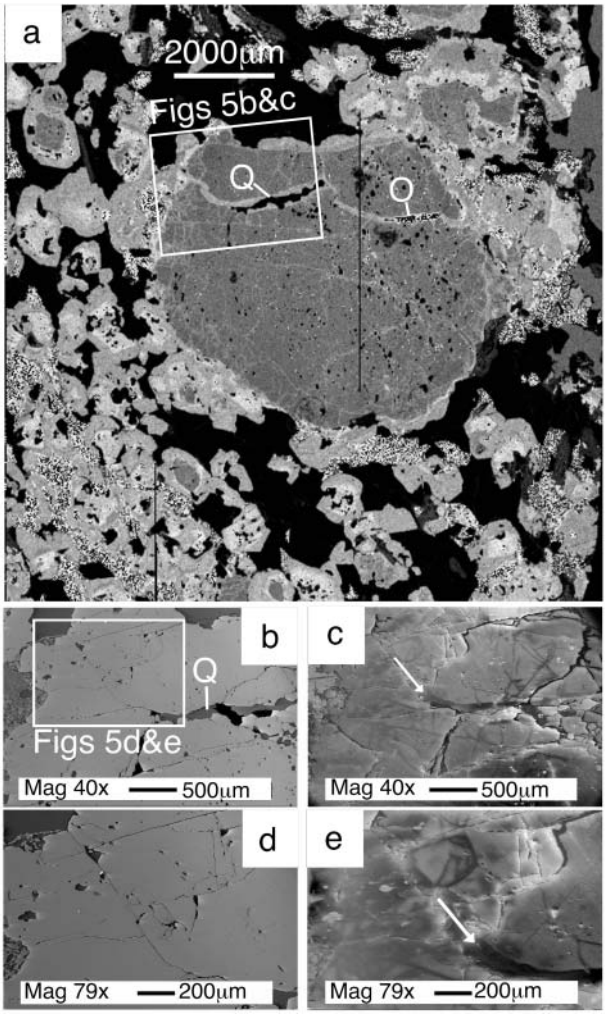

FIGURE 5. X-ray compositional map, BSE, and CCI images of large garnet. **(a)** Ca map, showing large low-Ca core, narrow high-Ca rim and network of narrow high-Ca linear features, interpreted as healed cracks, including a broader band cored by quartz (Q) and omphacite (O). Dark vertical line is a transient probe failure. White rectangle shows area covered in b and c. White arrow indicates where corresponding CCI-dark lineament dies out in c. **(b**, **d)** BSE images of parts of the grain shown in a. White rectangle in b shows area covered in d and e. Q = quartz. **(c, e)** CCI images corresponding to b and d, respectively. White arrows show where the broad CCI-dark band, corresponding to the high-Ca band in a, dies out. For **b-d**, the vacuum was 0.4 Torr and the working distance 10.2 mm.

DISCUSSION

GSE image contrast in the garnets examined here reveals features independent of late fractures in the crystals, and closely matches fine-scale, major-element compositional variation. These features could not be resolved by BSE imaging. Attempts to image them using a conventional cathode luminescence detector in the ESEM also showed no image contrast. The images took a few seconds to acquire, in contrast to the X-ray compositional maps, which took several hours. The spatial resolution and sharpness of detail are also superior to compositional mapping even using the cold-field emission SEM, because the activation volume for X-ray generation is larger than that for near-surface GSE emission (Griffin 2000). The speed of image acquisition and spatial resolution make charge-contrast imaging a potentially very useful tool for reconnaissance studies of the internal microstructure and compositional variation of garnets. Hot-cathode luminescence imaging can produce images of crack-like features and growth

zones in garnets that are similar to those shown here (Schertl 2003). The CCI method has a better signal-to-noise ratio than CL (Griffin 2000), and may have superior spatial resolution, again due to a smaller activation volume. However, like CL there is a time constant involved with GSE imaging, so emission may not be from the area of current activation, thus reducing resolution.

The mechanism responsible for the GSE image contrast remains a somewhat open question. If, following Griffin (2000), charge-contrast images show the distribution of the density of lattice defects, several possibilities exist. Some features of the images shown above may suggest some possibilities worthy of pursuing further. First of all, the association of darker image areas with growth zoning suggests that the property of the garnet controlling image contrast results from the growth process. Rapid growth of new, crack-healing garnet may be indicated by the fact that, in spite of the apparent shattering of the garnet, it has maintained its shape and does not seem to have disaggregated, despite lying in a matrix with a strong L-tectonite fabric. Hence, the new crack-healing garnet grew quickly enough to prevent disaggregation during continuing extension of the matrix. Such rapid growth could have resulted in a high concentration of lattice defects. Alternatively, a high defect concentration might have arisen from dislocations resulting from crystal-plastic deformation of the garnet, as described by Prior et al. (2000).

Close correspondence of the GSE-dark areas with compositional variation (Fig. 5) suggests that image contrast results from cationic substitutions, but normal homovalent substitutions among major elements (Ca, Mg, Fe, Mn) are unlikely to create charge-trapping defects. Also, the correlation of image-dark areas with the more Ca-rich garnet is not perfect, indicating that image contrast is not directly related to major element compositional variation, but some feature closely associated with it. Substitution of Y^{3+} and REE^{3+} for divalent cations on the garnet x-sites may result in creation of vacancies, for example $3M^{2+} = 2(Y, REE)^{3+} + \square$ (Bea et al. 1997; Quartieri et al. 1999a, 1999b). Such vacancies may act as charge-trapping point defects. Vacancies may also be created by incorporation of hydroxyl ions, for example in the hydrogarnet substitution $^{IV}Si^{4+} + 4O^{2-} = {}^{IV}\square + 4OH^{-}$, creating a tetrahedrally co-ordinated vacancy surrounded by four protonated O atoms (Rossman and Aines 1991). Small concentrations of structurally bound hydroxyl are known to be quite common in natural, mantle-derived and UHP metamorphic garnets (Langer et al. 1993; Beran et al. 1993; Bell et al. 1995; Rossman 1996; Matsyuk et al. 1998; Andrut et al. 2002). Incorporation of hydroxyl in the garnets described here would be consistent with the concept of precipitation of crack-healing garnet aided by an aqueous fluid. Beran (1996) concluded that incorporation of defect hydroxyl in nominally anhydrous, close-packed silicate structures requires associated vacancies in the cation sites, for example vacancies at octahedral Cr or Al sites (Andrut et al. 2002), or on tetrahedral sites associated with substitution of octahedral Ti for tetrahedral Si and octahedral Al (Khomenko et al. 1994). Spatial variability of hydroxyl concentration within individual garnet grains has been resolved using FTIR spectroscopy by Khomenko et al. (1994). A similar type of coupled substitution in zircon in which Y and REE replace Zr, balanced by hydroxyl and vacancy defects, has been proposed as the source of cathodoluminescent emission (Ohnenstetter et al. 1991). Shannon et al. (1992) reported that the dielectric properties of ceramic cordierite are influenced by mobile hydrous components, leading to increased dielectric loss. If the same applies to silicate garnets, this may help to explain the varying charge-trapping characteristics observed in the specimens described here. A priority for further research will be detection of any hydroxyl component and associated trace-element substitutions.

If the CCI-dark features result from defect concentrations leading to enhanced near-surface charge-trapping, one might expect them to give a brighter image. However, the image contrast has been shown to be reversible, and depends on the balance of trapping and dissipation rates vs. the scan rate. At relatively fast scan rates a defect-rich area will tend to experience a slower charge build-up than a defect-poor area, so defect-rich areas will appear darker (Fig. 8 in Watt et al. 2000). Hence, the darker appearance of the crack-seal and overgrowth garnet is quite consistent with a higher defect concentration.

Concluding remarks

Gaseous secondary-electron imaging of polished surfaces of natural aluminosilicate garnets from an eclogite in the environmental scanning electron microscope under conditions of low chamber gas pressure reveals richly detailed image contrast (Charge-Contrast Imaging), in line with similar observations from other silicates by Watt et al. (2000). Image features show close correspondence with spatial variation in major-element composition, indicating that the CCI-dark garnet is a late generation of eclogite-facies garnet precipitated by accretion to the old garnet rim, and as crack-fills. Image contrast may not be directly related to major-element composition, and it is speculated that it may be related to growth-related defects, and/or to concentrations of vacancies resulting from substitutions of trace elements coupled to hydroxyl incorporation, the latter offering the intriguing possibility that charge-contrast images may be a method for obtaining high-resolution images of internal hydroxyl distribution in garnet crystals. It may also offer a method for imaging the distribution of REE dopants and/or hydroxyl in synthetic, ceramic garnets. Whatever the cause of the image contrast, the speed and high resolution of charge-contrast imaging makes it a potentially very useful technique for rapid reconnaissance studies of fine-scale garnet microstructure. Future studies should concentrate on elucidating the causes of image contrast in terms of lattice defect types, compositional variation, and dielectric properties, fine-tuning the operating conditions to maximise resolution and image clarity.

Acknowledgments

Thanks to Margaret Corrigan for technical assistance with the SEM at the University of Paisley Thin Film Centre. SJC acknowledges funding from a EU Access to Research Infrastructures Programme to carry out microprobe analyses and compositional mapping at the Bayreuth GeoInstitut, University of Bayreuth, Germany, and assistance with analysis from Detlef Krausse. F. Placido and D.A. Carswell are thanked for constructive comments on earlier drafts of the manuscript. The authors are grateful to reviewers B. Griffin and D. Prior for their constructive and helpful comments.

References cited

Andrut, M., Wildner, M., and Beran, A. (2002) The crystal chemistry of birefringent natural uvarovites. Part IV. OH defect incorporation mechanisms in non-cubic garnets derived from polarized IR spectroscopy. European Journal

of Mineralogy, 14, 1019–1026.
Baroni, T.C., Griffin, B.J., Browne, J.R., and Lincoln, F.J. (2000) Correlation between charge contrast imaging and the distribution of some trace level impurities in gibbsite. Microscopy and Microanalysis, 6, 49–58.
Bea, F., Montero, P., Garuti, G., and Zacharini, F. (1997) Pressure-dependence of rare earth element distribution in amphibolite- and granulite-grade garnets. A LA-ICP-MS study. Geostandards Newsletter, 21, 253–270.
Bell, D.R., Ihinger, P.D., and Rossman, G.R. (1995) Quantitative analysis of OH in garnet and pyroxenes. American Mineralogist, 80, 465–474.
Beran, A. (1996) Defect hydroxyl in close-packed mineral structures. Physics and Chemistry of Minerals, 23, 306.
Beran, A., Langer, K., and Andrut, M. (1993) Single crystal infrared spectra in the range of OH fundamentals of paragenetic garnet, omphacite and kyanite in an eklogitic (sic) mantle xenolith. Mineralogy and Petrology, 48, 257–268.
Bryhni, I. and Griffin, W.L. (1971) Zoning in eclogite garnets from Nordfjord, West Norway. Contributions to Mineralogy and Petrology, 32, 112–125.
Carswell, D.A. and Cuthbert, S.J. (2003) Ultrahigh pressure metamorphism in the Western Gneiss Region of Norway. In D.A. Carswell & R. Compagnoni, Eds., Ultrahigh Pressure Metamorphism. EMU Notes in Mineralogy, 5, p. 51–73. Eotvos University Press, Budapest.
Carswell, D.A., Cuthbert, S.J., Krabbendam, M., Medaris, L.G. Jr., and Brueckner, H.K. (2003) Guidebook to the Field Excursions in the Nordfjord—Stadlandet—Almklovdalen Area. NGU Open Report no. 2002.056, Chapter 5, Part 2, p. 97–104. Norwegian Geological Survey, Trondheim, Norway.
Griffin, B.J. (1997) A new mechanism for the imaging of crystal structure in non-conductive materials: An application of charge-induced contrast in the environmental scanning electron microscope (ESEM). Microscopy and Microanalysis, 3 (supp. 2), 1197–1198.
Griffin, B.J. (1998) Electrons, ions and cathodoluminescence in the environmental SEM. Microscopy and Microanalysis, 4 (supp. 2), 290–291.
——— (2000) Charge contrast imaging of material growth and defects in environmental scanning electron microscopy—linking electron emission and cathodoluminescence. Scanning, 22, 234–242.
Harker, A.B., Howitt, D.G., DeNatale, J.F., and Flintoff, J.F. (1994) Charge-sensitive secondary electron imaging of diamond microstructures. Scanning, 16, 87–90
Hirsch, D.M., Prior, D.J., and Carlson, W.D. (2003) An overgrowth model to explain multiple, dispersed high-Mn regions in the cores of garnet porphyroblasts. American Mineralogist, 88, 131–141.
Hwang Shyh-Lung, Hwang, Pouyan Shen, Tzen Fu Yui, and Hao-Tsu Chu (2001) Defect microstructures as a potential indicator of extremely rapid and episodic exhumation of ultrahigh-pressure metamorphic rock: implication to continental collision orogens. Earth and Planetary Science Letters, 192, 57–63.
Khomenko, V.M., Langer, K., Beran, A., Koch-Muller, M., and Fehr, T. (1994) Titanium substitution and OH-bearing defects in hydrothermally grown pyrope crystals. Physics and Chemistry of Minerals, 20, 483–488.
Krogh, E.J. (1982) Metamorphic evolution of Norwegian country-rock eclogites, as deduced from mineral inclusions and compositional zoning in garnets. Lithos, 15, 305–321.
Langer, K., Robarik, E., Sobolev, N.V., Shatsky, V.S., and Wuyi, W. (1993) Single-crystal spectra of garnets from diamondiferous high-pressure metamorphic rocks from Kazakhstan: indications for OH^-, H_2O, and FeTi charge transfer. European Journal of Mineralogy, 5, 1091–1100.
Matsyuk, S.S., Langer, K., and Hösch, A. (1998) Hydroxyl defects in garnets from mantle xenoliths in kimberlites of the Siberian platform. Contributions to Mineralogy and Petrology, 132, 163–179.
Matthews, M., Harte, B., and Prior, D. (1992) Mantle garnets: A cracking yarn. Geochimica et Cosmochimica Acta, 56, 2633–2642.
Mohan, A., Khana N., Hwu, J., and Joy, D.C. (1998). Secondary electron imaging in the variable pressure electron microscope. Scanning, 20, 436–441.
Ohnenstetter, D., Cesbron, F., Remond, G., Caruba, R., and Claude, J.-M. (1991) Emissions de cathodoluminescence de deux populations de zircons naturels: tentative d'interpretation. Comptes Rendues de l'Academie des Sciences. Serie II, 641–647.
Prior, D.J. and Wheeler, J. (2002) Some garnet micro structures: an illustration of the potential of orientation maps and misorientation analysis in microstructural studies. Journal of Structural Geology, 24, 999–1011.
Prior, D.J., Wheeler, J., Brenker, F.E., Harte, B., and Matthews, M. (2000). Crystal plasticity of natural garnet: New microstructural evidence. Geology, 28, 1003–1006
Quartieri, S., Antonioli, G., Geiger, C.A., Artioli, G., and Lottici, P.P. (1999a) XAFS characterisation of the structural site of Yb in synthetic pyrope and grossular garnets. Physics and Chemistry of Minerals, 26, 251–256.
Quartieri, S., Chaboy, J., and Antonioli, G. (1999b) XAFS characterisation of the structural site of Yb in synthetic pyrope and grossular garnets. II: Xanes full multiple scattering calculations at the Yb L_I and L_{III} edges. Physics and Chemistry of Minerals, 27, 88–94.
Rossman, G.R. (1996) Studies of OH in nominally anhydrous minerals. Physics and Chemistry of Minerals, 23, 299–304.
Rossman, G.R. and Aines R.D. (1991) The hydrous components in garnets: Grossular-hydrogrossular. American Mineralogist, 76, 1153–1164.
Schertl, P. (2003) Cathodoluminescence petrography of UHP-metamorphic rocks from Dora Maira/Western Aps, Kokchetav/Kazakhstan and Sulu/China (abstract). In E. Eide (ed.) The Alice Wain Memorial West Norway Eclogite Field Symposium, Abstract Volume, pp. 129–130. NGU Open Report no. 2003.055. Geological Survey of Norway.
Shannon, R.D., Mariano, A.N., and Rossman, G.R. (1992) Effect of H_2O and CO_2 on dielctric properties of single crystal cordierite and comparison with polycrystalline cordierite. Journal of the American Ceramic Society, 75, 2395–2399.
Spear, F.S. and Daniel, C.G. (1998) Three-dimensional imaging of garnet porphyroblast sizes and chemical zoning: Nucleation and growth history in the garnet zone. Geological Materials Research, 1, 1–44.
Terry, M.P. and Heidelbach, F. (2004) Superplasticity in garnet from eclogite facies shear zones in the Haram Gabbro, Haramsoya, Norway. Geology, 32, 281–284.
Trepmann, C.A. and Stockhert, B. (2002) Cataclastic deformation of garnet: a record of synseismic loading and postseismic creep. Journal of Structural Geology, 24, 1845–1856.
Watt, G.R., Griffin, B.J., and Kinny, P.D. (2000) Charge contrast imaging of geological materials in the environmental scanning electron microscope. American Mineralogist, 85, 1784–1794.
Zamoryanskaya, M.V. and Pis'mennyi, V.A. (2000) Cathodoluminescence characterisation of defects in yttrium aluminium garnet doped with Nd. Inorganic Materials, 36, 620–624.

MANUSCRIPT RECEIVED DECEMBER 5, 2004
MANUSCRIPT ACCEPTED NOVEMBER 30, 2004
MANUSCRIPT HANDLED BY RICHARD KETCHAM